SLAC – PUB – 3850
ITP – 802
October 1985
(T/E)

ATOMIC ENHANCEMENTS IN THE DETECTION OF AXIONS

SAVAS DIMOPOULOS [‡] and GLENN D. STARKMAN [§]
Physics Department, Stanford University, Stanford, CA 94305

and

BRYAN W. LYNN [*]
Theory Group, Stanford Linear Accelerator Center,
Stanford University, Stanford CA 94305

ABSTRACT

Proposed bolometric and supercolloidal detectors can measure energy depositions of the order of atomic energies. At these energies, atomic bound state effects lead to great enhancements in the detection of absorbable weakly interacting particles. In this paper we compute these enhancements taking into account all Coulomb effects for nonrelativistic electrons. As an example, we show that solar axions could give event rates 10^4–10^5 times larger than published neutrino detector design capabilities. Thus, relatively small detectors might see solar axions.

Submitted to *Physical Review D*

---

[*] Work supported by Department of Energy, contract DE–AC03–76SF00515.

[‡] Work supported by National Science Foundation Grant PHY–83–10654.

[§] National Science and Engineering Research Council (Canada) Postgraduate Scholar.

INTRODUCTION

There are arguments in both theoretical elementary particle physics and astrophysics for the proliferation of neutral weakly interacting particles. On the theoretical side, gauge theories suggest the existence of many new particles: neutrinos, axions,[1] *etc.*Experimentally, astronomical observations suggest that the mass of the universe is dominated by dark matter which might be made of neutral weakly interacting particles. Because these particles tend to interact *so* weakly, we must rely on some enhancement mechanisms to detect them. For example, one suggested enhancement mechanism for detecting neutrinos relies on their coherent nuclear scattering;[2–6] this works well for neutrinos if the momentum transfers involved are less than 100 MeV.

Until now, detectors for weakly interacting particles, such as neutrinos, have been limited by high minimum energy deposition thresholds. However, recent progress in experimental techniques[3,5] has made feasible the measurement of energy depositions as small as atomic energies using supercolloidal and bolometric detectors. In this paper we show that, at these energies, atomic bound state effects lead to great enhancements ($\approx 10^6$) in the detection rates of weakly interacting particles which can be absorbed. As a simple example we work out the ionization of atoms by axions, but clearly this is applicable to other light scalar and pseudoscalar particles.

Atomic enhancements are quite familiar. A well-known example is the photoelectric effect, shown in Fig. 1. The photoelectric cross section per unit mass of, for example, silicon is 234 times larger than that of hydrogen around 1 keV photon energies. This is because silicon has electrons with binding energies of $\sim$ 1 keV; similar enhancements occur in any atom with keV electron binding energies.

Enhancements similar to those in the photoelectric effect occur for the ionization of atoms by absorption of axions. We call this process, depicted in Fig. 2,

the axioelectric effect or axionization. We expect such effects to be large for solar axions because their energy is comparable to atomic energies.

In a previous paper[7] we considered this process neglecting Coulomb effects for the outgoing electron. In this paper we include all such effects for the detector material. Thus the results of this paper supercede those of Ref. 7. We show that the rate of axionization could be four to five orders of magnitude larger than the published design capabilities of planned bolometric and supercolloidal neutrino detectors.[3,5]

AXIOELECTRIC EFFECT

The axioelectric effect is directly analogous to the photoelectric effect; a boson is absorbed by a bound electron, which is then ejected from the atom (Fig. 2).

In this section we calculate the rate for the axioelectric effect in the true physical situation of an electron in a detector. Such a nonrelativistic electron sees a background potential $V(\vec{r})$ due to the ion to which it is bound and the crystal in which the atom is embedded. $V(\vec{r})$ can thus be arbitrarily complicated and may depend on the experimental situation (external fields, *etc.*) The initial and final state Schroedinger wavefunctions $|i\rangle$ and $|f\rangle$ are eigenstates of the electron Hamiltonian

$$\mathcal{H} = \frac{p^2}{2m_e} + V(\vec{r}) \quad . \tag{1}$$

The matrix element for the photoelectric effect is obtained by studying the non-relativistic limit of the electron (ψ) — transverse photon ($\vec{A}$) coupling in QED

$$\mathcal{L}_{QED} = -e\,\bar{\psi}\,\vec{\gamma}\cdot\vec{A}\,\psi \quad , \tag{2}$$

$$\mathcal{M}_{photoelectric} \simeq -e\left\langle f\left|\frac{e^{i\vec{k}\cdot\vec{r}}}{\sqrt{2k}}\left[-i\,\frac{\vec{\epsilon}\cdot\vec{\nabla}}{m_e} + i\,\frac{\vec{\sigma}\cdot\vec{k}\times\vec{\epsilon}}{2m_e}\right]\right|i\right\rangle \quad . \tag{3}$$

The matrix element for the axioelectric effect comes from the nonrelativistic reduction of the coupling of the axion field (a) to the pseudoscalar electron current.

$$\mathcal{L} = 2X_e' \frac{m_e}{F}\, a\bar{\psi}\, i\gamma_5\, \psi \quad , \tag{4}$$

where X_e' is a constant of order unity[8] which Srednicki[9] argues argues is greater than one in the DFS model. In the following, we consider only light axions ($m_{axion} \ll k$) where k is the axion energy. The axioelectric matrix element follows from Eq. (4)

$$\mathcal{M}_{axioelectric} = -\left(\frac{2X_e' m_e}{F}\right) \left\langle f \left| \frac{e^{i\vec{k}\cdot\vec{r}}}{\sqrt{2k}} \frac{\vec{\sigma}\cdot\vec{k}}{2m_e} \right| i \right\rangle \quad .$$

If we make the dipole approximation $kr \ll 1$ and treat the final-state electron as a plane wave $|f> \sim exp\{i\vec{p}_f \cdot \vec{r}\}$, the result [Eq. (1)] in Ref. 7 follows with the approximation $p_f^2/(2m_e) \simeq k$. In this note we want to take into account the properties of the initial and final states in the actual physical situation in the detector material; the fact that the electron sees a background potential due to the ion and the detector crystal. Thus we write in the dipole approximation

$$\mathcal{M}_{photoelectric} \simeq -\frac{e}{\sqrt{2k}} \langle f \,|\, i\, k\, \vec{r}\cdot\vec{\epsilon}\,|\, i\rangle \quad , \tag{6}$$

where we have made use of the fact that $k = E_{final} - E_{initial}$ and that

$$\frac{\vec{\epsilon}\cdot\vec{p}}{m_e} = i\,[H, \vec{r}\cdot\vec{\epsilon}] \quad . \tag{7}$$

Similarly, we write

$$\mathcal{M}_{azioelectric} \simeq -\left(\frac{2X_e' m_e}{F}\right) \frac{1}{\sqrt{2k}} \left\langle f \left| i\vec{k}\cdot\vec{r}\, \frac{\vec{\sigma}\cdot\vec{k}}{2m} \right| i \right\rangle \quad . \tag{8}$$

Note that the first term in the expansion $exp\{i\vec{k}\cdot\vec{r}\} = 1 + i\vec{k}\cdot\vec{r} + \ + \ +$ has vanished in the axioelectric effect because for the true electron wavefunction $\langle f|i\rangle = 0$. Thus, it follows that

$$\sigma_{azioelectric} = \frac{\alpha_{axion}}{\alpha}\left(\frac{k}{2m_e}\right)^2 \sigma_{photoelectric} \tag{9}$$

$$\alpha_{axion} = \left(\frac{2X_e' m_e}{F}\right)^2 \frac{1}{4\pi} \quad . \tag{10}$$

Note that Eq. (9) is correct for all initial bound states (of angular momentum $L = 0, 1, \ldots$) in any shell as long as the electron is nonrelativistic and $k \ll m_e$. If we then take $\sigma_{photoelectric}$ from data, all complicated effects due to the presence of the ion and crystal (band structure, *etc.*), will automatically be taken into account in the axioelectric effect.

The standard theoretical lower bound from solar physics[10,11,12] on $F/2X_e'$, $F/2X_e' > 1.08 \times 10^7$ GeV, is obtained by requiring that the solar axion luminosity not exceed the photon luminosity.[13–16] Furthermore, cosmological arguments give an *upper* bound[17] of $F < 10^{12}$ GeV. In this paper we shall assume $F/2X_e' = 10^7$ GeV, but it must be remembered that the event rate goes as $(F/2X_e')^{-4}$.

EVENT RATES

For $F/2X_e' = 10^7$ GeV, the axionization event rates in various elements can be obtained by multiplying $\sigma_{azio}(k)$ of Fig. 3 with the solar axion flux calculated with solar temperature $T = 1$ keV (Fig. 4). Following Raffelt,[12] we take the solar flux to be entirely due to bremsstrahlung. In the previous paper,[7] Primakoff production was also considered, but Raffelt has shown that this is suppressed for the sun. In Fig. 5 we plot the events per kilogram per day per keV against the incoming axion energy. From these figures we see that the major contribution to the event rate comes from a narrow band between 1 keV and 10 keV. This is

because the solar axion flux falls off sharply above 10 keV, and the axioelectric cross section falls off sharply below 1 keV.

In Fig. 6 we plot the total number of events per kilogram per day as a function of the minimum experimentally observable incoming axion energy ω_{min}.

$$\left[\begin{array}{c}\text{Number of events}\\ \text{per kg per day}\end{array}\right] = \left[\begin{array}{c}\text{Number of atoms}\\ \text{per kg}\end{array}\right] \times \int_{\omega_{min}}^{\infty} \sigma_{axio}(\omega)\,\phi(\omega)\,d\omega \ , \quad (3)$$

where $\phi(\omega)$ is the solar axion flux[10,11,12] (see Fig. 4).

In Figs. 7 and 8 we plot the total events per kilogram per day for $\omega_{min} = 1$ keV for several elements spanning the periodic table. Note that the total event rate per kilogram per day is fairly constant for $Z \gtrsim 13$. This is probably because the number of electrons contributing to the axionization or photoionization cross section at a few keV grows approximately linearly with Z, for $Z \gtrsim 13$, while the number of atoms in a kilogram is roughly Z^{-1}. Thus the choice of detector material is not limited by event rate as long as $Z \gtrsim 13$.

In the table we give the integrated events per kilogram per day for electrons in silicon and germanium with $\omega_{min} = 1$ keV and compare them to the neutrino induced electron events calculated by the authors of Ref. 5. Note that bolometric detector design capabilities aim at detecting 10^{-3} to 10^{-4} events per kilogram per day, while the axioelectric effect will give up to eight events per kilogram per day. Our rates are comparable to the reactor antineutrino detection rates quoted in the table.

In Fig. 9, we plot the integrated number of events per kilogram per day in silicon (solid line) and germanium (dot-dashed line) with energy deposition greater than 1 keV as a function of the axion mass[8,9]

$$m_{axion} \simeq 7.2\ eV \left[\frac{10^7\ \text{GeV}}{F}\right] \ . \quad (4)$$

For comparison, we also plot the published solar neutrino detector design capabilities (dashed line).[3,5] Note that if these minimum design capabilities are met,

we will be sensitive to axion masses at least as small as 0.5 eV for $2X_e' = 1$ and 0.5 eV$/2X_e'$ in general.

It is therefore feasible either to detect solar axions or to set a laboratory lower bound on $F/2X_e'$ which is an order of magnitude better than the bound of 1×10^7 GeV and does not rely on the details of stellar models.[18]

CONCLUSIONS

In a previous[7] paper we studied the first example of how atomic enhancements can lead to detectable signals even from very weakly coupled particles, when the energy transfers are comparable to atomic energies. There we neglected Coulomb effects of the outgoing electron. Here we have included all such effects of the electron's interaction with the detector material and thus the results of this paper supercede those of Ref. 7. These atomic enhancements make it possible to have large rates for solar axion detection.

ACKNOWLEDGMENTS

It is a pleasure to thank David Ritson for illuminating conversations. We would also like to thank B Cabrera, M. Karliner, L. Krauss, J. Martoff, D. E. Morris, H. Quinn and R. Wagoner for valuable discussions.

REFERENCES

1. R. D. Peccei and H. R. Quinn, Phys. Rev. Lett. **3B**, 1440 (1977): Phys. Rev. **D16**, 1791 (1977). S. Weinberg, Phys. Rev. Lett. **40**, 223 (1978). F. Wilczek, Phys. Rev. Lett. **40**, 279 (1978). J. E. Kim, PHys. Rev. Lett. **43**, 103 (1979). M. A. Shifman, A. I. Vainshtein and V. I. Zakharov, Nucl. Phys. **B166**, 493 (1980). M. Dine, W. Fischler and M. Srednicki, Phys. Lett. **104B**, 199 (1981) J. E. Moody and F. Wilczek, Phys. Rev. **D30**, 130 (1984). Other axion detectors have been proposed by P. Sikivie, Phys. Rev. Lett. **51**, 1415 (1983); **52**, 695 (1984).

2. D. Z. Freedman, D. L. Tubbs and D. N. Schramm, Ann. Rev. Nucl. Sci. **27**, 167 (1977).

3. A. Drukier and L. Stodolsky, Phys. Rev. **D30**, 2295 (1984).

4. M. Goodman and E. Witten, Princeton University preprint.

5. B. Cabrera, L. Krauss and F. Wilczek, Phys. Rev. Lett. **55**, 25 (1985).

6. L. Krauss, M. Srednicki and F. Wilcek, U.C. Santa Barbara preprint ITP–85–58, Yale preprint UTRP–85–18. Submitted to Phys. Rev. Lett. A. De Rujula, S. L. Glashow and L. J. Hall, Harvard University preprint HUTP–85/A074 (1985).

7. S. Dimopoulos, G. D. Starkman and B. W. Lynn, Phys. Lett. **B167**, 145 (1986).

8. D. B. Kaplan, Nucl. Phys. **B260**, 215 (1985).

9. M. Srednicki, Nucl. Phys. **B260**, 689 (1985).

10. D. S. Dicus, E. W. Kolb, V. L. Teplitz and R.V.Wagoner, Phys. Rev. **D18**, 1829 (1978) and **D22**, 829 (1980). M. Fukujita, S. Watamura and M. Yoshimura, Phys. Rev. Lett. **48**, 1522 (1982).

11. L. M. Krauss, J. E. Moody and F. Wilczek, Harvard University preprint HUTP–84–A043.

12. G. G. Raffelt, 1985 Max Planck Institute (Munich) preprint MPI–PAE/PTh–51/85.

13. Speculative astrophysical arguments have been made which place more severe lower bounds on F: $F > 4 \times 10^7$ GeV (red giant cooling),[10] $F > 4 \times 10^9$ GeV (He ignition in red giants),[15] $F > 6 \times 10^8 - 3 \times 10^9$ GeV (x-ray pulsar cooling,[14] and $F > 10^9$ GeV (white dwarf cooling.)[16] All of the above arguments rely on the details of models of stars which are very different than the sun; the strongest bounds rely on a proper understanding of stellar evolution.

14. Lower bounds of $F > 6 \times 10^8 - 3 \times 10^9$ GeV have been obtained by N. Iwamoto [Phys. Rev. Lett. **53**, 1198 (1984)] and D. E. Morris [LBL report 18690 mc (1984)], from limits on axion cooling of x-ray pulsars. However, these calculations neglect possible internal and external heat sources and assume that the observed x-ray spectra are thermal and neglect the possibilities of nonthermal magnetospheric emission and internal heat sources; their results must therefore be considered speculative. Furthermore, note that the upper bound on the luminosities of the well-known x-ray sources SN 1006, Tycho and Cast is *below* the predictions of the standard cooling model [K. Nomoto and S. Tsurute, Ap. J. **250** (1981) 19. This suggests additional cooling mechanisms for x-ray sources including, possibly, axion emission.

15. D.S.P. Dearborn, D. N. Schramm, G. Steigman, Bartol Research Foundation preprint BA–85–54 (1985).

16. G. G. Raffelt, 1985 Max Planck Institute (Munich) preprint MPI–PAI/PTh–67/85.

17. J. Preskill, M. B. Wise and F. Wilczek, Phys. Lett. **120B**, 127 (1983). L. Abbot and P. Sikivie, Phys. Lett. **120B**, 133 (1983). M. Dine and W. Fischler, Phys. Lett. **120B**, 137 (1983).

18. Note that for the interaction of a light ($m_\phi \ll 1$ keV) scalar ϕ with a scalar electron current $\mathcal{L} = \lambda \bar{e} e \phi$ the cross section for ionization via a process analogous to Fig. 2 is $\sigma_{scalarelectric} \simeq \lambda^2/(4\pi\alpha)\ \sigma_{photoelectric}$ including all Coulomb effects for nonrelativistic electrons. This does not suffer the suppression factor $(k/2m_e)^2$ so that bounds on $\alpha_{scalar} = \lambda^2/4\pi$ from the scalarelectric effect could be $\sim 10^6$ times stronger than those on α_{axion} from the axioelectric effect for energy depositions of 1 keV. This also applies for theoretical astrophysical bounds on α_{scalar} analogous to those in Refs. 10–16 from the theoretical limits on light scalar emission from stars. It is obvious that similar enhancements occur for the absorption of any light boson ($m \ll 1$ keV) of any spin such as new vector particles or even gravitons whose energy is 1 keV.

TABLE

Event rates in a bolometric detector. The rates for the solar neutrino and reactor antineutrino induced events have been obtained from Ref. 5. Note that the solar axion induced event rates from any atom with $Z \gtrsim 13$ can be comparable to those computed in Ref. 5 for reactor antineutrinos.

Event rates in a bolometric detector	Events/kg/day
Recoil electrons from solar $pp\nu$'s on Si	1.0×10^{-3} 1.5×10^{-4}
Solar axion events on Si and Ge with energy deposition ≥ 1 keV for $F/2X'_e = 10^7$ GeV	Si 5.4 Ge 7.6

Figure Captions

Figure 1. Photoionization cross section per kilogram for H (dots), C (dot-dashes), Si (dashes) and Pb (solid). Note that for a photon energy of 1 keV there is an enhancement of about 10^3 for Si relative to H. Further, for both Si and Pb, the cross section for smaller photon energies is enhanced by a factor of $\approx 10^4$ relative to large photon energies due to atomic effects.

Figure 2. The axioelectric effect.

Figure 3. Axionization cross section per kilogram for C (dots), Si (dot-dashes), Ge (dashes) and Pb (solid). Note again that for axion energies of 1 keV there is an enhancement of about 10^3 for Si relative to H, and that the cross section at low energies is enhanced relative to the cross section at high energies by $\approx 10^4$.

Figure 4. The flux of solar axions on earth for solar temperature $T = 1$ keV. The flux is entirely due to bremsstrahlung.

Figure 5. Solar axion events per kilogram per day per keV for C (dots), Si (dot-dashes), Ge (dashes) and Pb (solid).

Figure 6. Integrated axion events per kilogram per day as a function of the minimum axion energy ω_{min} for C (dots), Si (dot-dashes), Ge (dashes) and Pb (solid). Note that the effect increases with Z for low Z then stabilizes for $Z \gtrsim 13$.

Figure 7. Integrated axion events per kilogram per day as a function of the minimum axion energy ω_{min} for H (light dots), Li (dots), Al (dot-dashes), Fe (dashes) and Pu (solid). Note that the scale is different from that of Fig. 6. Note also that for $Z \gtrsim 13$, the effect changes by only a factor 1.5 over a very wide range of the periodic table.

Figure 8. Integrated axion events per kilogram per day for $\omega_{min} = 1$ keV versus Z throughout the periodic table up to plutonium. Note that the effect grows linearly with Z up to $Z \simeq 13$ and then stabilizes. Therefore, the event rate does not place a constraint on the choice of detector material.

Figure 9. Integrated axion events with $E_{min} > 1$ keV per kilogram per day in Si (dots) and Ge (dot-dashes) versus axion mass for $2X'_e = 1$. Note that for the published design capabilities of 1.5×10^{-4}/kg day for Si detectors, we are sensitive to $m_a = 0.5$ eV$/2X'_e$.

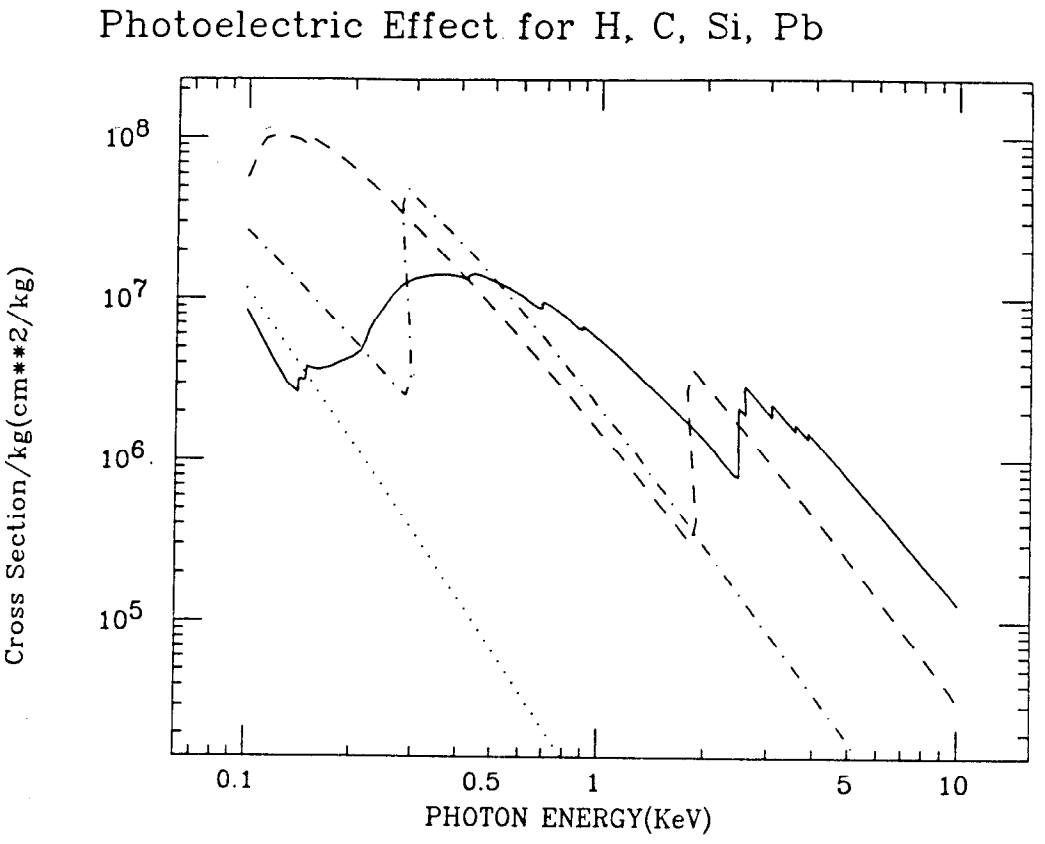
Photoelectric Effect for H, C, Si, Pb
Cross Section/kg(cm**2/kg)
10^8
10^7
10^6
10^5
0.1
0.5
1
5
10
PHOTON ENERGY(KeV)

Figure 1

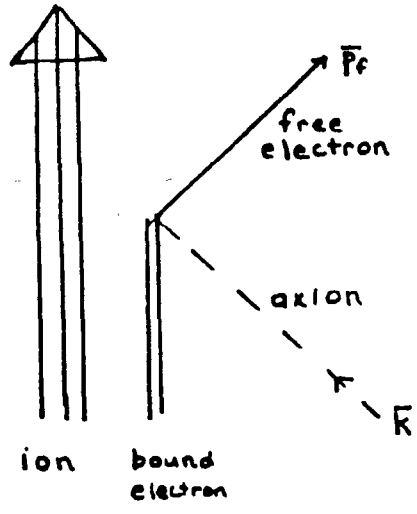

Figure 2

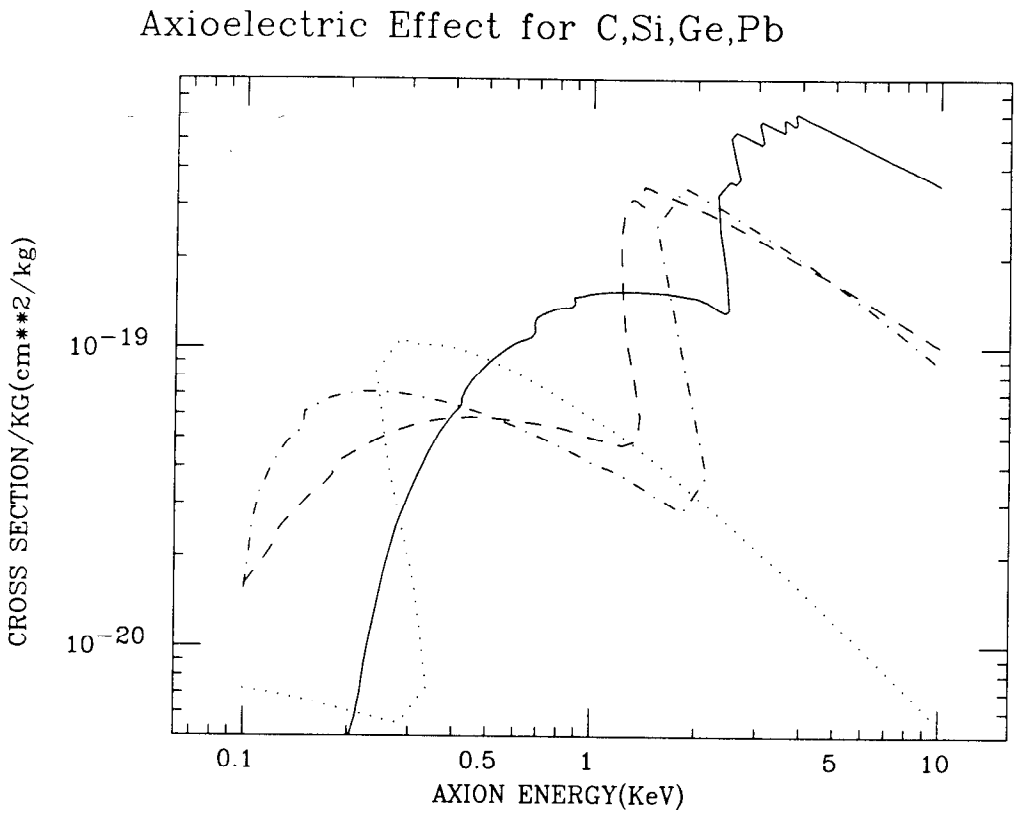
Axioelectric Effect for C,Si,Ge,Pb
CROSS SECTION/KG(cm**2/kg)
10^{-19}
10^{-20}
0.1
0.5
1
5
10
AXION ENERGY(KeV)

Figure 3

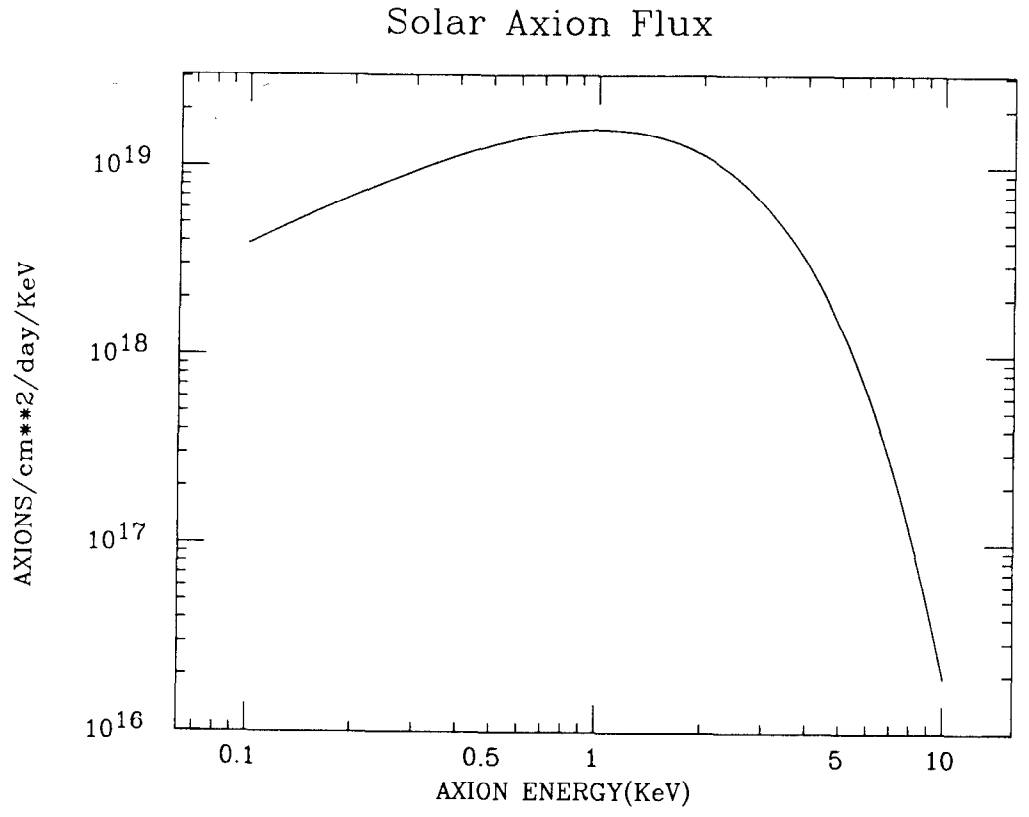
Solar Axion Flux
AXIONS/cm**2/day/KeV
10^{19}
10^{18}
10^{17}
10^{16}
0.1
0.5
1
5
10
AXION ENERGY(KeV)

Figure 4

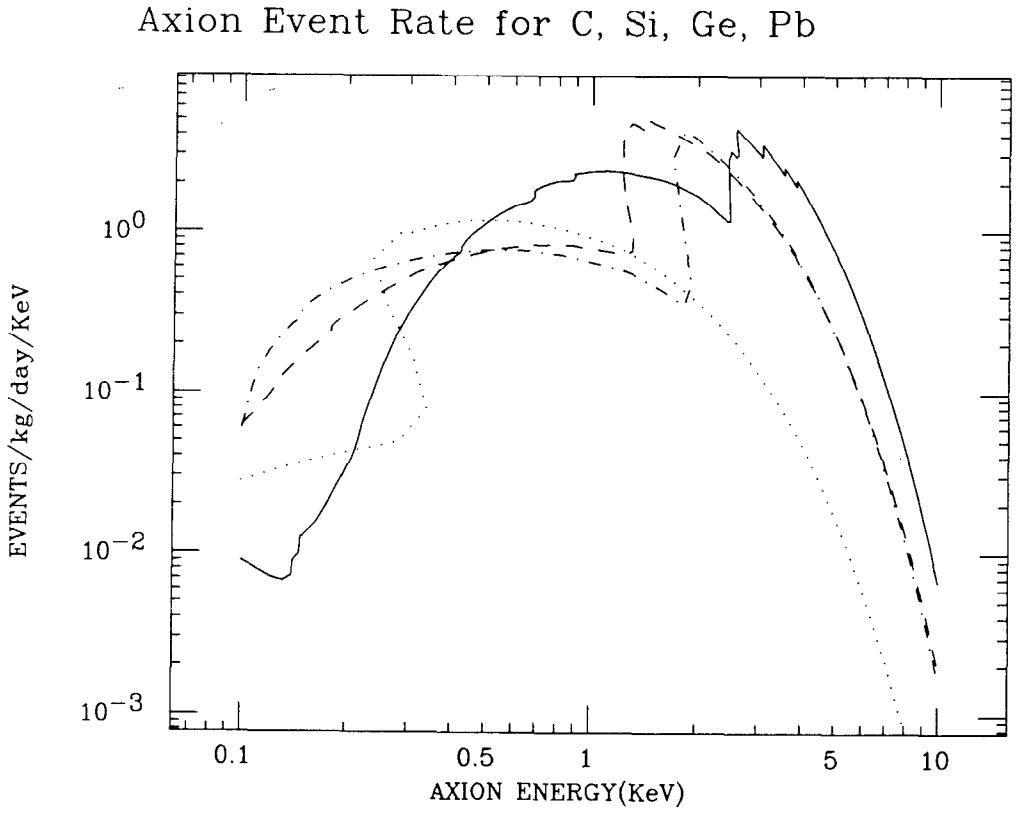
Axion Event Rate for C, Si, Ge, Pb
EVENTS/kg/day/KeV
10^0
10^{-1}
10^{-2}
10^{-3}
0.1
0.5
1
5
10
AXION ENERGY(KeV)

Figure 5

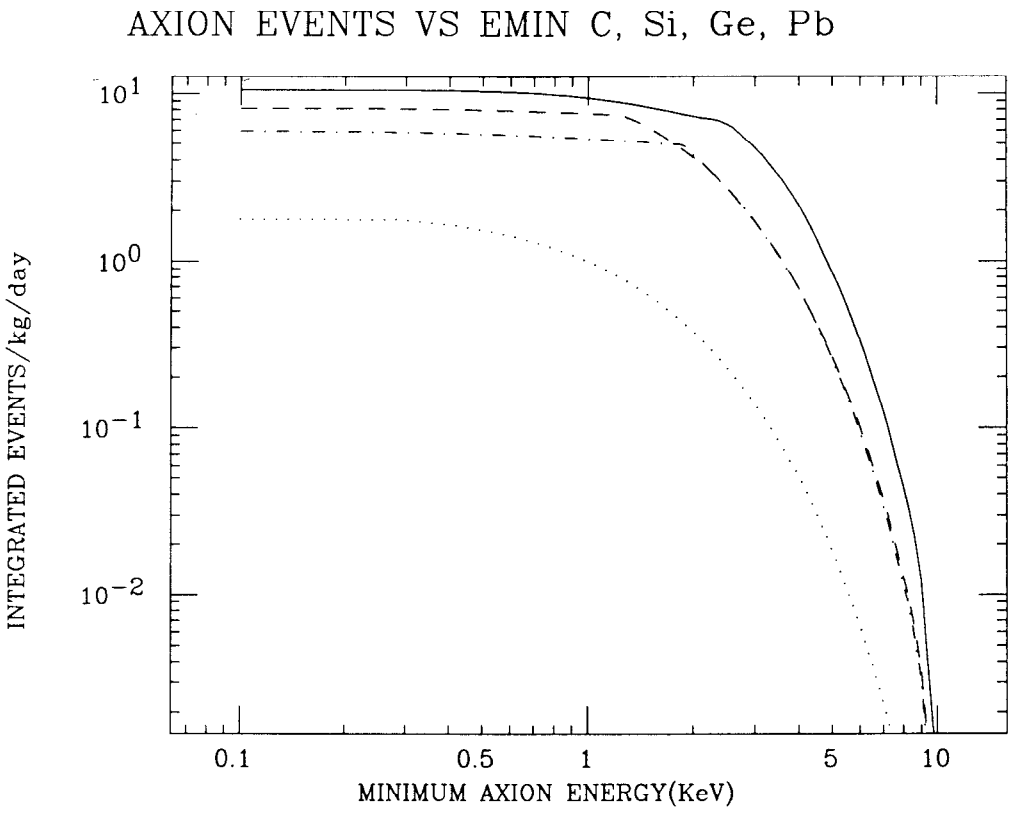
AXION EVENTS VS EMIN C, Si, Ge, Pb
INTEGRATED EVENTS/kg/day
10^1
10^0
10^{-1}
10^{-2}
0.1
0.5
1
5
10
MINIMUM AXION ENERGY(KeV)

Figure 6

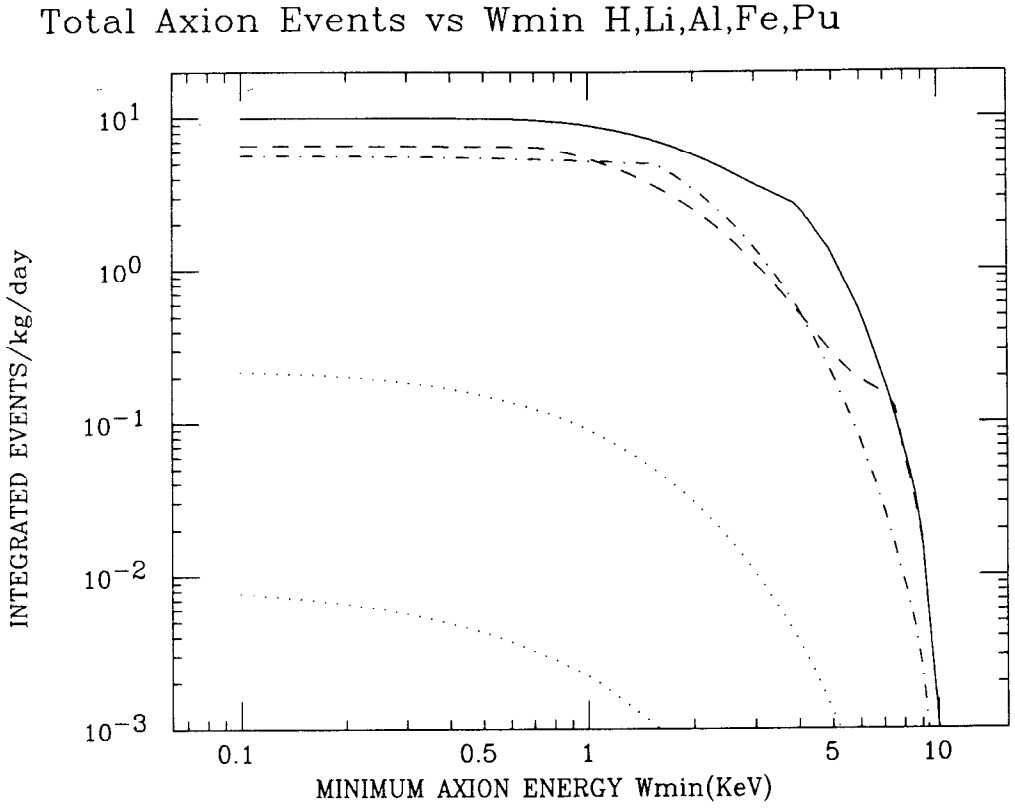
Total Axion Events vs Wmin H,Li,Al,Fe,Pu
INTEGRATED EVENTS/kg/day
10^1
10^0
10^{-1}
10^{-2}
10^{-3}
0.1
0.5
1
5
10
MINIMUM AXION ENERGY Wmin(KeV)

Figure 7

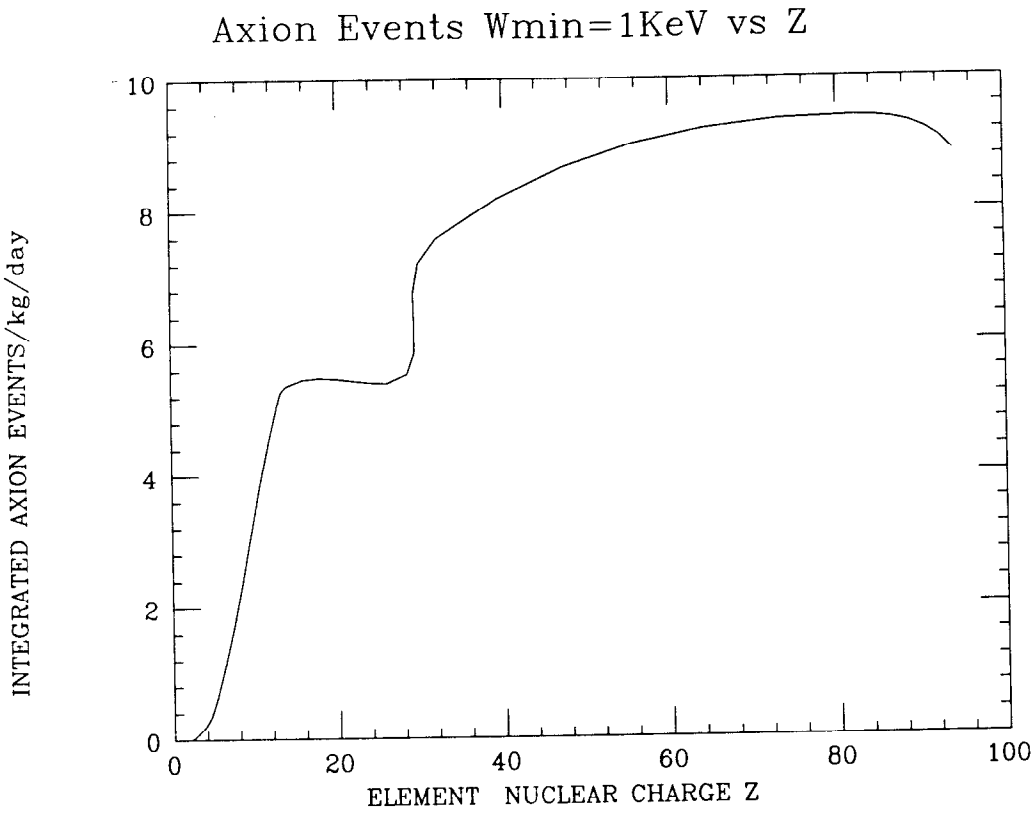
Axion Events Wmin=1KeV vs Z
INTEGRATED AXION EVENTS/kg/day
0
2
4
6
8
10
0
20
40
60
80
100
ELEMENT NUCLEAR CHARGE Z

Figure 8

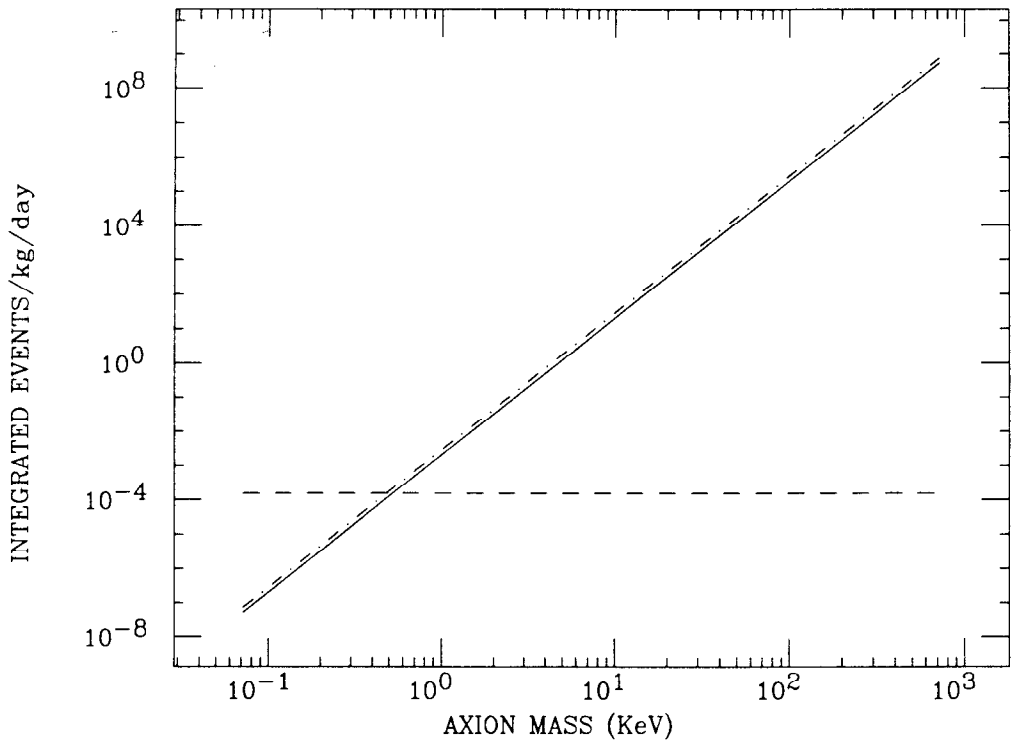
Integrated Events (Wmin=1KeV) vs Axion Mass
INTEGRATED EVENTS/kg/day
10^{8}
10^{4}
10^{0}
10^{-4}
10^{-8}
10^{-1}
10^{0}
10^{1}
10^{2}
10^{3}
AXION MASS (KeV)

Figure 9